10736 *Inorg. Chem.* **2010**, *49*, 10736–10743
DOI: 10.1021/ic101904j

Inorganic Chemistry
Article

Synthesis and Structures of $Pb_3O_2(CH_3COO)_2 \cdot 0.5H_2O$ and $Pb_2O(HCOO)_2$: Two Corrosion Products Revisited

Catherine M. Mauck,[†] Titus W. P. van den Heuvel,[†] Michaela M. Hull,[†] Matthias Zeller,[‡] and Catherine M. Oertel*,[†]

[†]*Department of Chemistry and Biochemistry, Oberlin College, 119 Woodland Street, Oberlin, Ohio 44074, United States, and* [‡]*Department of Chemistry, Youngstown State University, 1 University Plaza, Youngstown, Ohio 44555, United States*

Received September 16, 2010

Reactions of carboxylic acids with lead play an important role in the atmospheric corrosion of lead and lead−tin alloys. This is of particular concern for the preservation of lead-based cultural objects, including historic lead−tin alloy organ pipes. Two initial corrosion products, $Pb_3O_2(CH_3COO)_2 \cdot 0.5H_2O$ (**1**) and $Pb_2O(HCOO)_2$ (**2**), had been identified through powder diffraction fingerprints in the Powder Diffraction File, but their structures had never been determined. We have crystallized both compounds using hydrothermal solution conditions, and structures were determined using laboratory and synchrotron single-crystal X-ray diffraction data. Compound **1** crystallizes in $P\bar{1}$, and **2** in *Cccm*. These compounds may be viewed as inorganic−organic networks containing single and double chains of edge-sharing Pb_4O tetrahedra and have structural similarities to inorganic basic lead compounds. Bond valence sum analysis has been applied to the hemidirected lead coordination environments in each compound. Atmospheric exposure experiments contribute to understanding of the potential for conversion of these short-term corrosion products to hydrocerussite, $Pb_3(CO_3)_2(OH)_2$, previously identified as a long-term corrosion product on lead-rich objects. Each compound was also characterized by elemental analysis, thermogravimetric analysis and differential scanning calorimetry (TGA-DSC), and Raman spectroscopy.

Introduction

Atmospheric corrosion is a significant cause of deterioration of cultural artifacts made from lead and lead-rich alloys, including coins and organ pipes.[1−6] This damage is frequently observed when objects are kept in a wooden storage or display box or in proximity to a wooden case and wind system in an organ. As wood ages, hydrolysis of hemicellulose contained in cell walls leads to emission of acetic acid, and other small molecules, including formic acid, are released through additional processes.[7,8] In laboratory exposure experiments, these organic acids have been shown to be corrosive to pure lead and to lead-rich lead−tin alloys.[9−14] This degradation poses a threat to objects that are valued as documents of cultural, musical, and technological history, and a more complete understanding of the mechanism of the corrosion process is needed.

The corrosivity of acetic and formic acids toward lead-rich samples has been related to their ability to dissolve the otherwise protective nanoscale PbO layer that forms on metallic lead in oxygen-containing environments.[10,11,14] Under conditions of normal atmospheric humidity, the metal surface is covered with several monolayers of water,[15] providing a solvent for dissolution of acid vapors and carbon dioxide and subsequent breakdown of the oxide. In electrochemical corrosion, oxidation of the metal at an anodic site is accompanied by reduction of atmospheric oxygen at a

*To whom correspondence should be addressed. E-mail: catherine.oertel@oberlin.edu.

(1) Carradice, I. A.; Campbell, S. A. *Stud. Conserv*. **1994**, *39*, 100–106.
(2) Niklasson, A.; Langer, S.; Arrhenius, K.; Rosell, L.; Bergsten, C. J.; Johansson, L. G.; Svensson, J. E. *Stud. Conserv*. **2008**, *53*, 24–40.
(3) Chiavari, C.; Martini, C.; Prandstraller, D.; Niklasson, A.; Johansson, L. G.; Svensson, J. E.; Aslund, A.; Bergsten, C. J. *Corros. Sci*. **2008**, *50*, 2444–2455.
(4) Green, L. In *Conservation of Metals: Problems in the Treatment of Metal-Organic and Metal Inorganic Composite Objects*. Proceedings of the International Restorer Seminar, Veszprém, Hungary, July 1−10, 1989; Jaro, M., Ed.; National Center of Museums: Budapest, 1990.
(5) Mattias, P.; Maura, G.; Rinaldi, G. *Stud. Conserv*. **1984**, *29*, 87–92.
(6) Sharma, V. C.; Shankar Lal, U.; Singh, T. *Stud. Conserv*. **2003**, *48*, 203–209.
(7) Arni, P. C.; Cochrane, G. C.; Gray, J. D. *J. Appl. Chem*. **1965**, *15*, 305–313.
(8) Gibson, L. T.; Watt, C. M. *Corros. Sci*. **2010**, *52*, 172–178.
(9) Niklasson, A.; Johansson, L. G.; Svensson, J. E. *Corros. Sci*. **2008**, *50*, 3031–3037.
(10) Niklasson, A.; Johansson, L. G.; Svensson, J. E. *J. Electrochem. Soc*. **2007**, *154*, C618–C625.
(11) Niklasson, A.; Johansson, L. G.; Svensson, J. E. *J. Electrochem. Soc*. **2005**, *152*, B519–B525.
(12) Oertel, C. M.; Baker, S. P.; Niklasson, A.; Johansson, L. G.; Svensson, J. E. *J. Electrochem. Soc*. **2009**, *156*, C414–C421.
(13) Tetreault, J.; Cano, E.; van Bommel, M.; Scott, D.; Dennis, M.; Barthes-Labrousse, M. G.; Minel, L.; Robbiola, L. *Stud. Conserv*. **2003**, *48*, 237–250.
(14) Tetreault, J.; Sirois, J.; Stamatopoulou, E. *Stud. Conserv*. **1998**, *43*, 17–32.
(15) Leygraf, C.; Graedel, T. E. *Atmospheric Corrosion*; Wiley-Interscience: New York, 2000.

Published on Web 10/20/2010

cathodic site.[15] The resulting hydroxide ions create a basic environment in the electrolyte on the metal surface. The salts that precipitate from the electrolyte and accumulate as corrosion products are therefore frequently oxide and hydroxide compounds. X-ray diffraction analysis of corrosion films formed on deteriorated organ pipes has identified hydrocerussite [$Pb_3(CO_3)_2(OH)_2$] and cerussite [$PbCO_3$] as principal corrosion products.[3] In laboratory experiments in which lead and lead−tin alloy samples were exposed to organic acid vapors, phase identification showed basic lead acetate [$Pb_3O_2(CH_3COO)_2 \cdot 0.5H_2O$] (**1**), basic lead formate [$Pb_2O(CHO_2)_2$] (**2**), and plumbonacrite [$Pb_{10}O(OH)_6(CO_3)_6$], as initial corrosion products that most likely convert to the more stable carbonate-based products over longer periods of time.[9−11,14] The structures of plumbonacrite,[16] hydrocerussite,[17] and cerussite[18] have been determined, but those of the basic lead carboxylate products have never been solved. While **1** and **2** have been identified by powder X-ray diffraction (PXRD) fingerprints,[19,20] their crystal structures have not been reported.

The structures of a number of inorganic basic lead compounds, those containing oxide or hydroxide anions as well as complex inorganic anions, have been reported, including carbonates,[16,21,22] halides,[23] nitrates,[24−27] phosphates,[28] and selenates.[29,30] While some are naturally occurring minerals, diffraction quality crystals of others have been prepared using hydrothermal and high-temperature methods. Recently, hydrothermal synthesis has been used to prepare basic lead compounds containing oxygen-donating ligands such as isophthalate,[31,32] 1,3,5-benzenetricarboxylate,[33] maleate,[34] and proline-*N*-methyl-phosphonate.[35] Solution syntheses have also led to basic lead compounds containing methoxide[36] and thiolate[37] ligands. Here we report on the hydrothermal synthesis and structural characterization of basic lead acetate and basic lead formate. We have also studied the thermal behavior of these compounds and have investigated their conversion to the long-term corrosion product hydrocerussite.

Experimental Section

General Information. PbO (Aldrich), $Pb(CH_3COO)_2 \cdot 3H_2O$ (EM Science), and formic acid (Baker) were used as received. Reactions were carried out in 23 mL Teflon cups enclosed in stainless steel autoclaves (Parr). Room temperature powder X-ray diffraction (PXRD) patterns were collected on a Rigaku Ultima IV diffractometer with CuK_α radiation. A low-temperature (100 K) PXRD pattern was obtained through the 11-BM mail-in service at Argonne National Laboratory, where the sample was examined using synchrotron radiation tuned to 0.4121 Å. Thermogravimetric analysis (TGA) and differential scanning calorimetry (DSC) were conducted using a TA Instruments SDT 2960 Simultaneous DSC-TGA. Samples were heated to 600 °C at a ramp rate of 5 °C/min under breathing-quality air at a flow rate of 10 mL/min. Raman spectra were collected on a Thermo NXR Raman module associated with a Thermo/Nicolet 6700 FT-IR. Solid samples were examined in tubes 5 mm in diameter, and the 1064 cm^{-1} excitation laser was operated at a power of 0.4 W. Elemental analysis was conducted by Robertson Microlit Laboratories, Madison, NJ.

Synthesis. Compound **1** was synthesized using a modification of the method reported by Kwestroo and Langereis.[19] $Pb(CH_3COO)_2 \cdot 3H_2O$ (1.94 g, 5.1 mmol) was dissolved in 10 mL of deionized H_2O in a small beaker, and PbO (2.27 g, 10 mmol) was added. The resulting slurry was sonicated for 20 min, transferred to a 23 mL Teflon cup, and bubbled with nitrogen gas for 15 min. The reaction vessel was then sealed in an autoclave and placed in a 120 °C oven for 12 h. The vessel was allowed to cool to room temperature on the benchtop. The reaction mixture contained colorless, needle-like crystals, most of which were bundled and clumped with one another. Crystals for single-crystal X-ray analysis were taken directly from the mother liquor and placed under oil. To isolate bulk powder samples, the product mixture was transferred to test tubes and spun down using a centrifuge. The supernatant was removed and the solid dried under vacuum, without heating, in an Abderhalden drying pistol for at least 12 h before being transferred to a desiccator for storage. Yield 1.59 g (41%). Predicted (found) for $C_4H_7O_{6.5}Pb_3$: C 6.15% (6.06%), H 0.90% (0.80%), Pb 79.6% (78.4%). Raman (cm^{-1}): 2923 (C−H stretch), 1543 and 1411 (C−O stretch), 1347 (CH_3 deformation), 929 and 913 (C−C stretch), 666 and 648 (OCO deformation), 613 (OCO rocking), 371 and 287 (Pb−O stretch).

For synthesis of compound **2**, a stock solution of 4.72 M formic acid was prepared by performing a 5-fold dilution of concentrated acid in deionized water. PbO (0.738 g, 3.3 mmol), 5 mL deionized H_2O, and 0.7 mL of the formic acid stock solution (3.3 mmol) were combined. The mixture was sonicated and bubbled with nitrogen gas as for **1**. The reaction vessel was sealed in an autoclave and placed in a 110 °C oven for 12 h. The vessel was allowed to cool on the benchtop. Colorless, block-like crystals were removed from the mother liquor for single-crystal X-ray diffraction experiments. The bulk solid was isolated and dried as for **1**. Yield 0.496 g (29%). Predicted (found) for $Pb_2C_2H_2O_5$: C 4.61% (4.60%), H 0.38% (0.38%), Pb 79.6% (77.8%). Raman (cm^{-1}): 2835 (C−H stretch), 1342 (C−O stretch), 1060 (C−H bend), 758 (OCO deformation), 282 (Pb−O stretch).

Crystal Structure Determination. Diffraction data at 100 K for **1** (denoted **1a**) were collected at Beamline 11.3.1 at the Advanced Light Source (Lawrence Berkeley National Laboratory) using

(16) Krivovichev, S. V.; Burns, P. C. *Mineral. Mag.* **2000**, *64*, 1069–1075.
(17) Martinetto, P.; Anne, M.; Dooryhee, E.; Walter, P.; Tsoucaris, G. *Acta Crystallogr., Sect. C: Cryst. Struct. Commun.* **2002**, *58*, I82–I84.
(18) Chevrier, G.; Giester, G.; Heger, G.; Jarosch, D.; Wildner, M.; Zemann, J. *Z. Kristallogr.* **1992**, *199*, 67–74.
(19) Kwestroo, W.; Langereis, C. *J. Inorg. Nucl. Chem.* **1965**, *27*, 2533–2536.
(20) de Wolff, P. *ICDD Grant-in-Aid*; Technisch Physische Dienst: Delft, The Netherlands, 1964.
(21) Krivovichev, S. V.; Burns, P. C. *Mineral. Mag.* **2000**, *64*, 1063–1068.
(22) Krivovichev, S. V.; Burns, P. C. *Mineral. Mag.* **2000**, *64*, 1077–1087.
(23) Krivovichev, S. V.; Siidra, O. I.; Nazarchuk, E. V.; Burns, P. C.; Depmeier, W. *Inorg. Chem.* **2006**, *45*, 3846–3848.
(24) Krivovichev, S. V.; Li, Y. P.; Burns, P. C. *J. Solid State Chem.* **2001**, *158*, 78–81.
(25) Li, Y. P.; Krivovichev, S. V.; Burns, P. C. *J. Solid State Chem.* **2001**, *158*, 74–77.
(26) Li, Y. P.; Krivovichev, S. V.; Burns, P. C. *J. Solid State Chem.* **2000**, *153*, 365–370.
(27) Kolitsch, U.; Tillmanns, E. *Mineral. Mag.* **2003**, *67*, 79–93.
(28) Krivovichev, S. V.; Burns, P. C. *Z. Kristallogr.* **2003**, *218*, 357–365.
(29) Krivovichev, S. V.; Avdontseva, E. Y.; Burns, P. C. *Z. Anorg. Allg. Chem.* **2004**, *630*, 558–562.
(30) Kim, S. H.; Yeon, J.; Halasyamani, P. S. *Chem. Mater.* **2009**, *21*, 5335–5342.
(31) Yang, E. C.; Li, J.; Ding, B.; Liang, Q. Q.; Wang, X. G.; Zhao, X. J. *CrystEngComm* **2008**, *10*, 158–161.
(32) Zhang, L.; Qin, Y. Y.; Li, Z. J.; Lin, Q. P.; Cheng, J. K.; Zhang, J.; Yao, Y. G. *Inorg. Chem.* **2008**, *47*, 8286–8293.
(33) Zhang, L.; Li, Z. J.; Lin, Q. P.; Qin, Y. Y.; Zhang, J.; Yin, P. X.; Cheng, J. K.; Yao, Y. G. *Inorg. Chem.* **2009**, *48*, 6517–6525.
(34) Bonhomme, F.; Alam, T. M.; Celestian, A. J.; Tallant, D. R.; Boyle, T. J.; Cherry, B. R.; Tissot, R. G.; Rodriguez, M. A.; Parise, J. B.; Nyman, M. *Inorg. Chem.* **2005**, *44*, 7394–7402.
(35) Sun, Z. G.; Cui, L. Y.; Liu, Z. M.; Dong, D. P.; Meng, L.; Chen, H.; Zhang, L. C.; Zhu, Z. M.; You, W. S. *Inorg. Chem. Commun.* **2006**, *9*, 1121–1124.
(36) Shi, Y. J.; Xu, Y.; Chen, X. T.; Xue, Z. L.; You, X. Z. *Eur. J. Inorg. Chem.* **2002**, 3210–3213.
(37) Eichhofer, A. *Eur. J. Inorg. Chem.* **2005**, 1683–1688.

Table 1. Refinement Data for Compounds **1** and **2**

data	**1a**	**1b**	**2**
empirical formula	$C_4H_7O_{6.50}Pb_3$	$C_4H_7O_{6.50}Pb_3$	$C_2H_2O_5Pb_2$
wavelength (Å)	0.77490	0.71073	0.71073
temperature (K)	100(2)	296(2)	100(2)
crystal system	triclinic	triclinic	orthorhombic
space group	$P\bar{1}$	$P\bar{1}$	*Cccm*
a (Å)	7.2427(9)	7.2637(16)	9.3955(15)
b (Å)	11.5314(15)	11.548(3)	10.8276(17)
c (Å)	13.5236(18)	13.778(3)	5.8133(9)
α	112.322(2)	113.354(3)	
β	101.107(2)	100.108(3)	
γ	90.740(2)	90.270(3)	
V (Å^3)	1020.6(2)	1041.1(4)	591.39(16)
ρ (g·cm^{-3})	5.081	4.981	5.845
Z	2	2	4
μ (mm^{-1})	60.984	48.396	56.806
θ range for data collection	3.14°−34.26°	1.64°−31.34°	2.87°−28.25°
completeness	99.4%	99.6% (to 28°)	100.0%
data/restraints/parameters	6214/3/230	6230/0/237	409/15/37
GOF on F^2	0.993	1.134	1.289
R indices $[I > 2\sigma(I)]^a$	$R_1 = 0.0374$, $wR_2 = 0.0783$	$R_1 = 0.0354$, $wR_2 = 0.0949$	$R_1 = 0.0340$, $wR_2 = 0.1029$
R indices (all data)^a	$R_1 = 0.0668$, $wR_2 = 0.0896$	$R_1 = 0.0586$, $wR_2 = 0.1213$	$R_1 = 0.0341$, $wR_2 = 0.1030$
largest diff. peak and hole (e Å^{-3})	2.006 and −1.858	2.184 and −1.840	4.910 and −4.119

^{a} $R_1 = \sum||F_o| - |F_c||/\sum|F_o|$, $wR_2 = [\sum w(F_o^2 - F_c^2)^2/\sum w(F_o^2)^2]^{1/2}$.

synchrotron radiation tuned to $\lambda = 0.7749$ Å. A D8 goniostat equipped with a Bruker APEXII CCD detector was employed. Single crystal X-ray diffraction at 296 K for **1** (denoted **1b**) and at 100 K for **2** was performed on a Bruker AXS SMART APEX CCD system using MoK_α laboratory radiation. For each data set, data integration and unit cell determination were performed using SAINT.[38] Absorption corrections were performed using SADABS for **1** and TWINABS for **2**. The structures were solved using direct methods and refined by full-matrix least-squares on F_o^2 using SHELXTL.[39] All non-hydrogen atoms were refined anisotropically. In structures **1b** and **2**, refinement was completed with hydrogen atoms constrained to ride on carrying atoms. In **1a**, water O−H distances were restrained to 0.84 Å and H···H distances to 1.35 Å.

Refinement data for the two compounds are summarized in Table 1. Data listed under **1a** resulted from the low-temperature, synchrotron analysis of **1**, while those under **1b** came from the room-temperature, laboratory experiment. An initial structural model for **1**, based on laboratory data collected at 100 K, featured a unit cell with a volume of 509.28(18) Å^3 containing two disordered acetate ligands in its asymmetric unit. The correct structure, determined through reexamination at ambient temperature in a laboratory experiment and at 100 K with synchrotron radiation, is a double-volume supercell with four unique acetate ligands in positions corresponding to the disordered positions in the initial model. In both **1a** and **1b**, several of the light atom ADPs showed large correlations because of the pseudosymmetry. Selected pairs of atoms were thus constrained to have identical ADPs.

The crystal under investigation for compound **2** was found to be nonmerohedrally twinned. The orientation matrices for the two components were identified using the program Cell Now,[40] and the two components were integrated using SAINT. The twin operation is a 180.0° rotation about the reciprocal axis −0.996 1.000 0.000; the exact twin matrix identified by the integration program was 0.13996 −0.86013 −0.00030, −1.14027 −0.13971 0.00078, −0.00027 0.00007 −1.00010. The structure was solved and refined using only the non-overlapping reflections of the primary component below a *d*-spacing threshold of 0.75 Å.

Exposure Studies. Desiccator exposure studies were used to determine the effects of exposure to humid air on **1** and **2**. A saturated solution of sodium chloride in water (200 mL) was placed in the bottom of a desiccator to generate an atmosphere of 75% relative humidity (RH) at 23 °C.[41] Approximately 100 mg of **1** or **2** was placed in an open glass vessel with a fritted glass bottom and suspended in the desiccator without contacting the solution. The desiccator was sealed and placed in an insulated, thermostatted box maintained at 23 °C. The exposures were carried out for two weeks (336 h). At the end of each exposure, the sample was removed, dried over silica gel for at least 12 h, and characterized by PXRD.

Results and Discussion

Syntheses. The hydrothermal preparation of single crystals of **1** was carried out using a modification of a previously reported method in which lead acetate and lead oxide were reacted in water at room temperature.[19] While a polycrystalline powder formed at room temperature, heating the reaction mixture to above the normal boiling point of water was necessary to provide sufficient solubility for formation of single crystals. It was observed that polycrystalline samples of **1** can also be prepared using reaction of acetic acid and PbO in a 2:3 molar ratio, and the preparation of **2** was designed using this direct action of the organic acid on PbO. For each compound, phase purity of the bulk powder was verified by comparison with PXRD patterns available in the Powder Diffraction File (PDF, 18-1740 for **1** and 14-0831 for **2**) and with patterns calculated from newly obtained single-crystal data (Supporting Information, Figures S4−S8). In both preparations, unreacted PbO and hydrocerussite, $Pb_3(CO_3)_2(OH)_2$, appeared as part of the product mixture in initial trials. Three modifications of the synthetic procedure were critical to preparing phase-pure products. Bubbling reaction slurries with nitrogen gas prior

(38) *SAINT, Bruker Advanced X-Ray Solutions*; Bruker AXS, Inc.: Madison, WI, 1997−2003.
(39) Sheldrick, G. M. *Acta Crystallogr.* **2008**, *A64*, 112–122.
(40) Sheldrick, G. M. *Cell Now*; University of Göttingen: Göttingen, Germany, 2005 and Bruker AXS, Inc.: Madison, WI, 2005.
(41) Greenspan, L. *J. Res. Natl. Bur. Stand., Sect. A* **1977**, *81*, 89–96.

to heating helped to reduce carbonate contamination through displacement of carbon dioxide in the water. Sonication of reaction mixtures promoted reaction of PbO even at room temperature and minimized unreacted material remaining at the end of the reaction. Sonication followed by bubbling with nitrogen also led to less carbonate contamination than resulted after bubbling alone. Finally, isolating the products through centrifugation and drying under vacuum was important in obtaining carbonate-free products. Isolating products through filtration resulted in increased carbonate contamination, presumably because of increased exposure to atmospheric carbon dioxide.

Phase-pure powder of **1** could also be prepared using a 2:3 mixture of ethanol and deionized water as the solvent in place of pure deionized water. The reactant ratio and reaction temperature were not changed. Under these conditions, the product yield (93%) was considerably higher than with use of water alone, but diffraction-quality single crystals were not formed, and examination by light and scanning electron microscopy showed that crystallites within the powder were not as well shaped. While crystallites formed in water were rod-like or needle-like, those formed in the mixed solvent were irregular. Addition of ethanol to the solvent appears to reduce the solubility of **1**, increasing the yield but compromising crystal quality.

Comparison of Powder and Single-Crystal Data for Compound 1. As noted above, the phase purity of synthesized powders of **1** and **2** was determined in part through comparison with PXRD patterns calculated from single-crystal data. Initially, it was noted that there was not ideal agreement between the experimental pattern for **1**, collected at room temperature, and the pattern calculated from structure **1a**, determined at 100 K. Structure **1b** was determined at room temperature, and a powder pattern was obtained at 100 K. With this new experimental data, good agreement was attained between experimental and calculated PXRD peak positions at both 100 K and ambient temperature (Supporting Information, Figures S6−S7). The single crystal structures indicate that there is no change in symmetry as the sample is warmed or cooled. Rather, there are adjustments in cell parameters, particularly in the *c*-axis length and in the cell angles, that lead to notably different powder patterns at the two temperatures. For **2**, there was good agreement between an experimental PXRD pattern collected at room temperature and that calculated from the structure determined at 100 K, indicating smaller structural adjustments with temperature than for **1** (Supporting Information, Figure S8).

Differences in peak intensities were noted between calculated and experimental patterns for **1** at ambient temperature. In particular, several peaks belonging to the 00*l* series were more intense in the experimental pattern. Scanning electron microscopy imaging revealed a rod-like or needle-like habit for crystals of **1** even after grinding for powder diffraction, and it is likely that preferred orientation is a cause of differences in predicted and observed intensities. Indeed, in a room-temperature powder pattern of material grown from an ethanol−water mixture and exhibiting small, irregular crystallites, the intensities of peaks in the 00*l* series were in much better agreement with the calculated pattern (Supporting Information, Figure S7). Kwestroo and Langereis noted an enhancement of intensity in this same set of peaks and attributed it to preferred orientation, though they did not index the powder pattern.[19] Our new structure and the resulting indexing of the enhanced peaks therefore build on this previous work.

Comparison with Powder Diffraction File Entries. The single crystal structures that were determined for **1** and **2** show slightly different stoichiometries than those associated with the PDF entries containing the powder fingerprints. Card number 18-1740 contains the unindexed powder diffraction information for **1** recorded by Kwestroo and Langereis.[19] The formula is entered as $Pb(CH_3COO)_2 \cdot 2PbO \cdot H_2O$. We have chosen to express it as $Pb_3O_2(CH_3COO)_2 \cdot nH_2O$ because, as will be shown in the structural discussion below, this is a better representation of the compound's structure. The room temperature powder pattern of hydrothermally synthesized basic lead acetate agrees very well with the reported pattern, but results from single crystal diffraction and thermogravimetric analysis indicate the presence of 0.5 water molecules per formula unit, not one molecule as indicated in the PDF entry. The powder used by Kwestroo and Langereis was prepared at room temperature and characterized by chemical analysis, though the method was not specified. It is reasonable that the higher temperature employed in the current work could result in a difference in extent of hydration. However, TGA analysis of powder newly synthesized at room temperature using the method of Kwestroo showed the same mass loss due to water as the hydrothermally prepared compound. The extent of hydration may be sensitive to other experimental details including handling and storage.

Card number 14-0831 provides an indexed powder pattern for a compound with the stoichiometry Pb(OH)(HCOO). The pattern, unit cell dimensions, and peak indexing are all in good agreement with what we have determined for compound **2**. Considering that the stoichiometry of the PDF entry, when multiplied by 2, can be rewritten as $Pb_2O(HCOO)_2 \cdot H_2O$, we see that it can be viewed as a hydrated form of **2**. A literature search did not reveal the synthetic method or further characterization of the compound described in the PDF, making it impossible to tell how its composition was established. The stoichiometry of our synthesized compound, established through single-crystal XRD, is supported by elemental analysis and thermogravimetric analysis and differential scanning calorimetry (TGA-DSC) (vide infra). Our new structure might revise an incorrect stoichiometry reported in the database or may represent a dehydrated form that is otherwise unchanged in structure.

The pattern reported in PDF 14-0831 was indexed to a C-centered orthorhombic cell. The space group is listed as C***(65), indicating that the cell was tentatively indexed as group 65, *Cmmm* but that the space group assignment was not certain. Our single crystal analysis found space group 66, *Cccm*. Of the 56 reflections reported in the PDF entry, only the 001 ($2\theta = 15.16°$, $I/I_o = 0.01$) and 061 ($2\theta = 53.55°$, $I/I_o = 0.08$) lines do not obey the reflection conditions of *Cccm*. With the exception of these two weak reflections, the pattern reported in 14-0831 can be indexed using the *Cccm* space group of our single crystal structure.

Structures. Both **1** and **2** have as their basic building blocks Pb_4O tetrahedra centered by μ_4 oxygen atoms. These tetrahedra share edges to form $Pb_3O_2^{2+}$ double chains in the

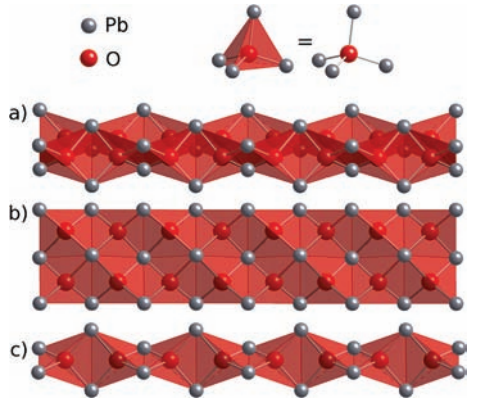

Figure 1. One-dimensional chains in **1** and **2**: (a) side view of $Pb_3O_2^{2+}$ double chain running in the [010] direction in **1**, (b) top view of $Pb_3O_2^{2+}$ double chain in **1**, (c) Pb_2O^{2+} single chain running in the [001] direction in **2**.

[010] direction in **1** (Figure 1 a,b) and Pb_2O^{2+} single chains in the [001] direction in **2** (Figure 1c). Both types of chains have been observed in lead-based minerals and synthesized compounds containing O^{2-} anions in addition to oxygen-containing complex anions.[42] Krivovichev et al. have pointed out that these one-dimensional chains may be seen as derivatives of the two-dimensional arrays of edge-sharing Pb_4O tetrahedra found in tetragonal PbO.[43] $Pb_3O_2^{2+}$ chains occur in compounds including $Pb_3O_2(SeO_3)$,[29,30] $Pb_3O_2Br_2$,[44] $Pb_3O_2(CO_3)$,[22] and the mixed-metal compound $Cu(Pb_3O_2)(OH)_2Cl_2$.[45] Examples of compounds containing Pb_2O^{2+} chains include $Pb_2O(SO_4)$, $Pb_4O(VO_4)_2$,[46] and $(Pb_2O)_2Cu(SO_4)(OH)_4 \cdot H_2O$.[47] However, extended structural components made up of inorganic Pb−O linkages have been rarely observed in basic lead compounds containing organic ligands, even though Pb_4O tetrahedra appear in some such hybrid compounds. One previous example is found in tribasic lead maleate hemihydrate, $[Pb_4O_3]C_2H_2(CO_2)_2 \cdot 0.5H_2O$, in which one-dimensional $Pb_4O_3^{2+}$ slabs are linked by maleate ligands.[34] By contrast, in $\{Pb_4O(bdc)_3(H_2O)\}_n$ (bdc = isophthalate), discrete Pb_4O units are linked through bridging carboxylate ligands but do not share edges or vertices with one another.[31,32] In $Pb_4O(O_3PCH_2-NC_4H_7-CO_2)_2$, pairs of Pb_4O tetrahedra share edges to form dimers that are linked into an extended structure by the organic ligands.[35]

In **1**, the Pb atoms that are part of the inorganic chains are further coordinated by oxygen atoms in acetate. Half of the acetate ligands act as bridges between adjacent chains, forming two-dimensional sheets (Figure 2a). The other acetate ligands coordinate multiple Pb atoms on one $Pb_3O_2^{2+}$ chain. In **2**, bridging formate ligands link the one-dimensional inorganic chains to form a three-dimensional network (Figure 2b).

Pb−O bonds in **1** were categorized as short (< 2.45 Å), intermediate (2.45−2.75 Å), and long (> 2.75 Å) using the classification of Krivovichev et al.[28,43] Considering the short and intermediate bonds only, Pb1 and Pb6 have

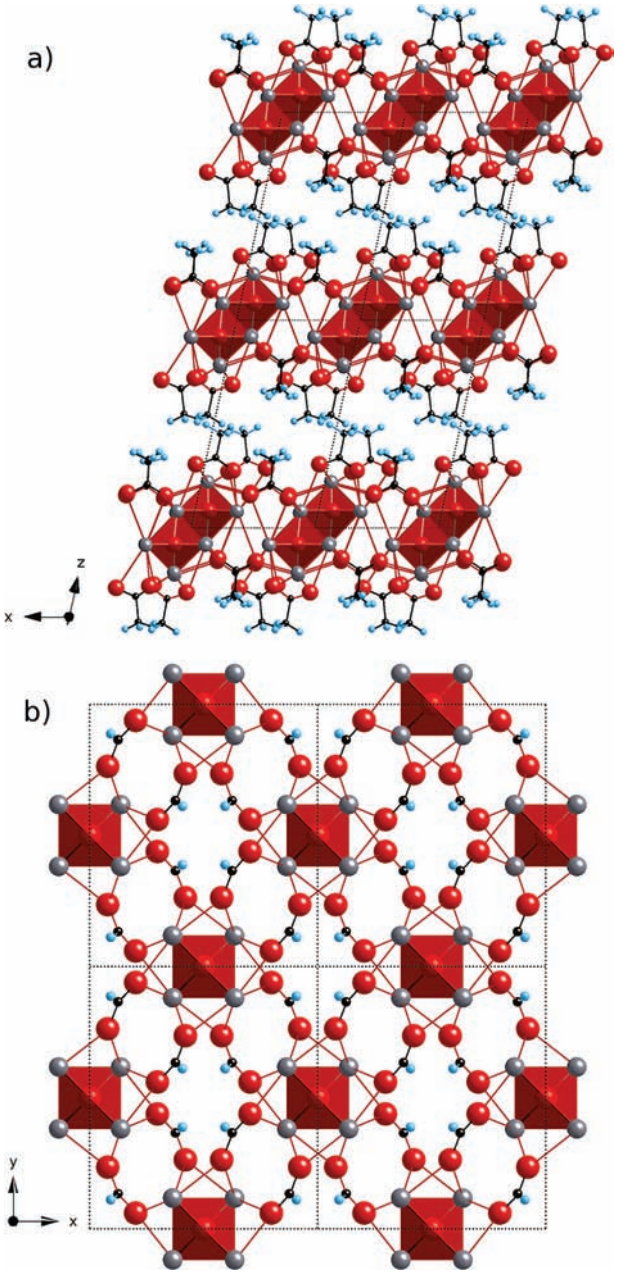

Figure 2. Extended structures of (a) **1** with $Pb_3O_2^{2+}$ chains viewed end-on and H_2O molecules omitted for clarity. Acetate ligands link the inorganic chains in the *x*-direction. (b) **2** with Pb_2O^{2+} chains viewed end-on. Formate ligands link the inorganic chains in the *x*- and *y*-directions. Lead atoms are shown in gray, oxygen atoms in red, carbon atoms in black, and hydrogen atoms in blue.

three-coordinate, trigonal pyramidal geometry (Figure 3 a,f). Pb2 and Pb5 have four-coordinate distorted disphenoidal, or "teeter-totter," geometry (Figure 3 b,e), and Pb3 and Pb4 are in four-coordinate, tetragonal pyramidal geometry (Figure 3 c,d). These geometries have previously been observed in the primary coordination spheres of lead carboxylate complexes.[48] Each of the sites is asymmetric, with all of the strong bonds directed toward one hemisphere, suggesting qualitatively that the $6s^2$ lone pair on Pb^{2+} is stereochemically active. When long bonds are also considered, the

(42) Siidra, O. I.; Krivovichev, S. V.; Filatov, S. K. *Z. Kristallogr.* **2008**, *223*, 114–125.
(43) Krivovichev, S. V.; Armbruster, T.; Depmeier, W. *J. Solid State Chem.* **2004**, *177*, 1321–1332.
(44) Noren, L.; Tan, E. S. Q.; Withers, R. L.; Sterns, M.; Rundlof, H. *Mater. Res. Bull.* **2002**, *37*, 1431–1442.
(45) Finney, J. J.; Graeber, E. J.; Rosenzweig, A.; Hamilton, R. D. *Mineral. Mag.* **1977**, *41*, 357–361.
(46) Krivovichev, S. V.; Burns, P. C. *Can. Mineral.* **2003**, *41*, 951–958.
(47) Kolitsch, U.; Giester, G. *Am. Mineral.* **2000**, *85*, 1816–1821.
(48) Davidovich, R. L.; Stavila, V.; Marinin, D. V.; Voit, E. I.; Whitmire, K. H. *Coord. Chem. Rev.* **2009**, *253*, 1316–1352.

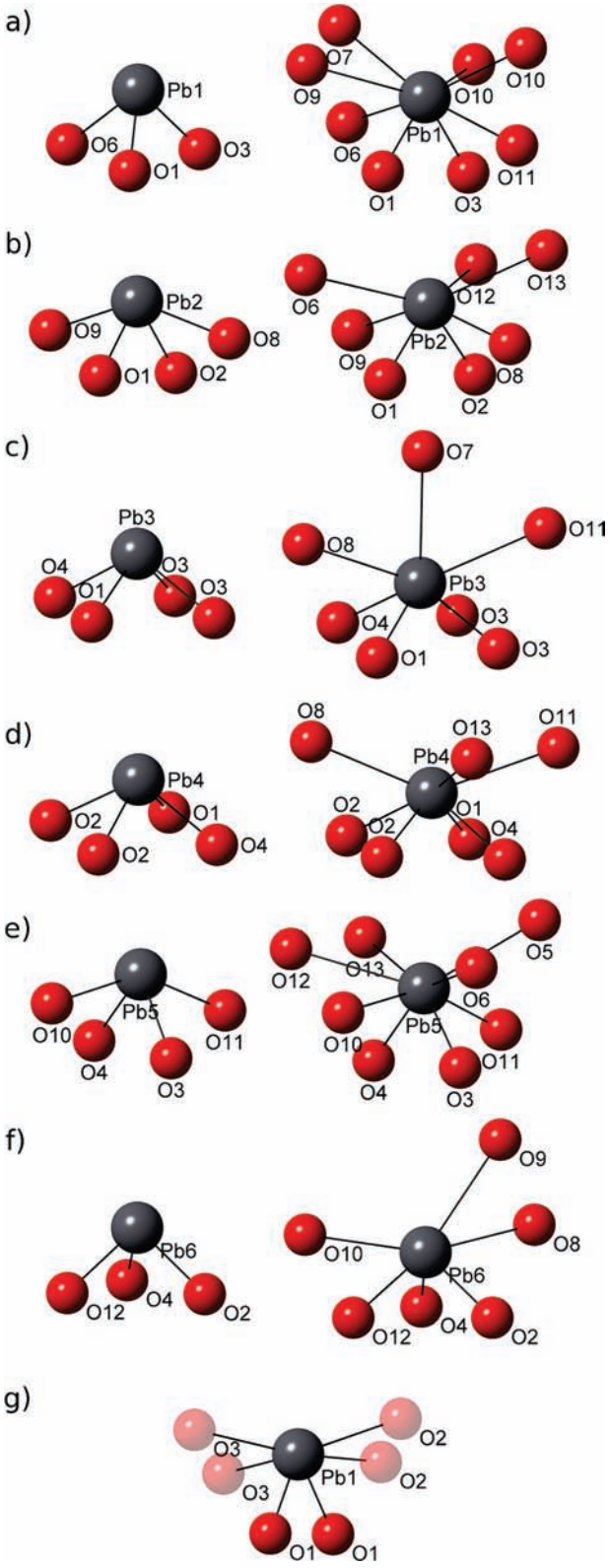

Figure 3. Coordination environments for Pb^{2+} showing short and intermediate bonds only (left) and all bonds (right): (a) Pb1 site in **1**, (b) Pb2 site in **1**, (c) Pb3 site in **1**, (d) Pb4 site in **1**, (e) Pb5 site in **1**, (f) Pb6 site in **1**, (g) Pb1 site in **2**. Flip disordered oxygen atoms with occupancies of 50% are shown as translucent spheres. Only one member of each disordered pair of atoms is shown.

resulting seven- and eight-coordinate geometries are irregular (Figure 3a−f). Long Pb−O contacts up to 3.316 Å in length are found for the six lead sites in **1**. The decision of which Pb−O contacts to consider as bonds was made based on examination of a histogram of Pb−O distances for each Pb site. Ranges of approximately 0.8−0.9 Å with no Pb−O contacts were found for Pb1, Pb2, Pb5, and Pb6, while gaps of 0.4 Å and 0.5 Å were found for Pb3 and Pb4, respectively. Distances above these gaps were not considered in the structural examination.

Bond-valence analysis (Supporting Information, Table S1) was carried out for each lead site in **1** using the parameters of Krivovichev and Brown, which have been shown to be most appropriate for Pb−O bonds.[49] Bond lengths from the low-temperature structure, **1a**, were used. Bond valence sums (BVS) for the six Pb sites range from 1.98 to 2.05 valence units (v.u.), very near the ideal value of 2.00 for Pb^{2+}.

In the coordination environment for the lead site in **2** (Figure 3g), no Pb−O contacts greater than 2.741 Å were found. Because of the flip disordering of the formate ligands, only half the positions for O(2) and O(3) are occupied for a given lead atom in the crystal. The O(1) sites are located on special positions and are fully occupied. The geometry is hemidirected and six-coordinate with two bonds to O(1) and two bonds each to O(2) and O(3), giving a BVS of 1.94 v.u. (Supporting Information, Table S1).

Thermal Decomposition. The thermal decompositions of **1** and **2** in air were studied using TGA-DSC (Supporting Information, Figures S9−S10). Compound **1** showed an endothermic mass loss of 1.2% below 100 °C. This decrease can be attributed to loss of water of crystallization and is in agreement with the 1.2% decrease predicted for 0.5 molecules of water per formula unit. A significant, exothermic transition, attributed to decomposition of the acetate ligands, occurred at approximately 350 °C. The associated mass loss was 14.5%, followed by an increase of 0.70% upon further heating. The orange-yellow residue remaining after heating of **1** to 600 °C was identified by PXRD as a mixture of tetragonal PbO (litharge) and orthorhombic PbO (massicot). The increase in mass above 400 °C is believed to be due to reoxidation of elemental Pb formed during the initial decomposition. The net loss of 13.8% is in reasonable agreement with the predicted loss of 13.1% for conversion of dehydrated **1** to PbO.

Under air, **2** showed no significant mass loss up to 250 °C, consistent with the characterization of this compound as an anhydrate. An endothermic decomposition associated with a mass loss of 14.4% occurred at approximately 260 °C, in agreement with the 14.2% loss expected for decomposition to PbO. The TGA trace suggested that this was a two-step process. On the basis of previous studies of thermal decomposition of lead formate, $Pb(CHOO)_2$, it is expected that the decomposition intermediate is a basic lead carbonate compound or a mixture of lead oxide and lead carbonate.[50,51] Using the temperature ramp rate of 5 °C/min, two small endothermic features were observed in the DSC trace between 400 and 600 °C, but only very broad mass changes could be seen. When this temperature range was reexamined using a ramp rate of 2 °C/min, a gradual mass increase was observed, followed by a distinct, endothermic mass loss of

(49) Krivovichev, S. V.; Brown, I. D. *Z. Kristallogr.* **2001**, *216*, 245–247.
(50) Baraldi, P. *Spectrochim. Acta, Part A* **1981**, *37A*, 99–102.
(51) Zhang, J.; Liu, Y. Y.; Zhang, Z. H.; Lv, X. C.; Sun, L. X.; Xu, F.; Tan, Z. C.; Zhang, T.; Sawada, Y. *J. Therm. Anal. Calorim.* **2007**, *89*, 643–647.

1.5% at 565 °C. PXRD analysis of a sample of **2** heated at 2 °C/min to 510 °C revealed a mixture of litharge and Pb_3O_4, while analysis of the residue after heating to 600 °C showed a mixture of the two polymorphs of PbO. The mass changes between 400 and 600 °C were therefore assigned to a gradual oxidation of PbO to Pb_3O_4 followed by a sharp decomposition back to PbO. A similar emergence and subsequent disappearance of Pb_3O_4 was previously reported as the result of decomposition of hydrocerussite, $Pb_3(CO_3)_2(OH)_2$, under flowing air.[52]

When heated to 600 °C under nitrogen, both **1** and **2** exhibited greater overall mass losses than when decomposed in air. The resulting residues were dark gray solids that were each identified by PXRD as a mixture of metallic lead and litharge with a small component of massicot. This contrasting behavior of a lead salt in nitrogen and air atmospheres, including reduction to elemental lead under nitrogen, was observed previously for lead acetate trihydrate.[53]

In situ thermodiffraction of **1** carried out under flowing air showed a marked change in the PXRD pattern between 60 and 80 °C. This temperature range corresponds with that over which water loss was observed by TGA-DSC. Preliminary data indicate that the dehydration is reversible, and detailed studies of the structure of the dehydrated compound and the kinetics and reversibility of the dehydration process are ongoing.

Roles of Basic Lead Acetate and Basic Lead Formate in Lead Corrosion. Both **1** and **2** are found as corrosion products when lead or lead-rich lead−tin alloys are exposed to atmospheres containing acetic and formic acids in laboratory exposure experiments.[10−12] However, neither is found in abundance as the product of the long-term corrosion of lead-based artifacts, which might take place over decades or centuries.[3] In a previous study, **1** was shown to undergo substantial conversion to hydrocerussite, $Pb_3(OH)_2(CO_3)_2$, upon exposure to humid air free of acetic acid vapor.[9] The experiment was done in a dynamic atmospheric exposure apparatus in which the sample was exposed to a continuous flow of humidified air over the two-week exposure period. The equilibrium reaction

$$Pb(CH_3COO)_2 \cdot 2PbO \cdot 0.5H_2O(s) + 2CO_2(g) + 1.5H_2O(g) \leftrightarrow Pb_3(OH)_2(CO_3)_2(s) + 2CH_3COOH(g) \quad (1)$$

was used to explain the observed transformation and to justify the requirements of atmospheric moisture and a low concentration of acetic acid vapor. An analogous reaction may be proposed for **2**:

$$3Pb_2O(CHOO)_2(s) + 4CO_2(g) + 5H_2O(g) \leftrightarrow 2Pb_3(OH)_2(CO_3)_2(s) + 6CHOOH(g) \quad (2)$$

To determine whether this reaction occurs to a significant extent, we carried out a two-week exposure in a chamber with a static, humidified atmosphere. Because of the difference in these conditions from those used previously by Svensson and co-workers,[9] we also exposed **1** under static conditions to be able to compare the behaviors of the two compounds. After the two-week static exposures, a PXRD pattern of each sample showed only a trace amount of hydrocerussite, and the starting compound remained as the dominant phase. The much lower extent of conversion of **1** in the static exposure chamber compared with the dynamic chamber may be explained by eq 1. In the dynamic exposure, products are favored because the continuous stream of humidified air brings CO_2 and H_2O to the sample and takes away acetic acid vapor that has been released. Like **1**, compound **2** showed conversion to hydrocerussite to a minimal extent under static conditions, and study of this process under a dynamic atmosphere and over longer periods of time could be the focus of future experiments.

Conclusions

Hydrothermal reactions proved to be an effective means of crystallizing basic lead acetate (**1**) and basic lead formate (**2**), both of which had previously been prepared only in polycrystalline form. Newly determined single-crystal structures show that the two compounds contain one-dimensional inorganic chains composed of edge-sharing Pb_4O tetrahedra and thus can be compared with a large family of inorganic lead compounds containing oxo-centered tetrahedra. These are, however, among the first hybrid materials containing extended lead oxide chains as well as organic linkages. Results of single-crystal X-ray diffraction and thermogravimetric analysis show different extents of hydration for the compounds as compared with their entries in the Powder Diffraction File. This outcome suggests that the extent of hydration for the compounds may be highly sensitive to synthetic and storage conditions, and preliminary results indicate that full dehydration of **1** occurs under mild heating. Further consideration of the interactions of these compounds with the environment, both in dehydration and in reactions with excess atmospheric moisture, will contribute to understanding of their properties and their role in corrosion of lead-based artifacts.

Acknowledgment. We acknowledge support from an NSF Discovery Corps Faculty Transfer Grant (CHE-0631522) and from Oberlin College. A Jean Dreyfus Boissevain Undergraduate Scholarship from the Camille and Henry Dreyfus Foundation supported the work of C.M.M. We thank Professor Jan-Erik Svensson, Professor Lars-Gunnar Johansson, Dr. Annika Niklasson, and Dr. James Kaduk for useful discussions and Ms. Gabrielle White-Dzuro for synthetic work. Samples for crystallographic analysis at the synchrotron were submitted through the SCrALS (Service Crystallography at Advanced Light Source) program. Crystallographic data were collected by Dr. Jeanette Krause Bauer at the Small-Crystal Crystallography Beamline 11.3.1 at the Advanced Light Source (ALS). The ALS is supported by the U.S. Department of Energy, Office of Energy Sciences Materials Sciences Division, under contract DE-AC02-05CH11231 at Lawrence Berkeley National

(52) Ciomartan, D. A.; Clark, R. J. H.; McDonald, L. J.; Odlyha, M. *J. Chem. Soc., Dalton Trans.* **1996**, 3639–3645.
(53) Mohamed, M. A.; Halawy, S. A.; Ebrahim, M. M. *Thermochim. Acta* **1994**, *236*, 249–262.

Laboratory. The low-temperature powder X-ray diffraction pattern was collected through the 11-BM mail-in program at Argonne National Laboratory. Use of the Advanced Photon Source at Argonne National Laboratory was supported by the U.S. Department of Energy, Office of Science, Office of Basic Energy Sciences, under Contract No. DE-AC02-06CH11357.

Supporting Information Available: Crystallographic information files (CIF) for structures **1a**, **1b**, and **2**; ellipsoid plots showing atom labeling schemes for structures **1a**, **1b**, and **2**; comparisons of calculated, experimental, and database powder patterns for compounds **1** and **2**; TGA-DSC traces for **1** and **2**; table of Pb−O bond lengths and bond valence sums. This material is available free of charge via the Internet at http://pubs.acs.org.